Organic donor-acceptor-donor trimers nanoparticles stabilized by amphiphilic block copolymers for photocatalytic generation of H_2

Thiago Guimarães, Alisha Khan, Hynd Remita, Jean-louis Bobet, Eric Cloutet

Organic donor-acceptor-donor trimers nanoparticles stabilized by amphiphilic block copolymers for photocatalytic generation of H_2

Thiago R. Guimarães,[1,3]* Alisha Khan,[2] Hynd Remita,[2] Jean-Louis Bobet,[3]* Eric Cloutet[1]*

[1] *Univ. Bordeaux, Laboratoire de Chimie des Polymères Organiques (LCPO, UMR 5629), CNRS, Bordeaux INP, F-33607 Pessac, France*
E-mail: thiago.guimaraes@u-bordeaux.fr, eric.cloutet@u-bordeaux.fr

[2] *Univ. Paris-Saclay, Institut de Chimie Physique (UMR 8000), CNRS, Orsay 91405, France*

[3] *Univ. Bordeaux, Institut de Chimie de la Matière Condensée de Bordeaux (ICMCB, UMR 5026), CNRS, Bordeaux INP, 33600 Pessac, France*
E-mail: jean-louis.bobet@icmcb.cnrs.fr

ABSTRACT

Photocatalytic generation of H_2 via water splitting emerges as a promising avenue for the next generation of green hydrogen due to its low carbon footprint. Herein, a versatile platform is designed to the preparation of functional π-conjugated organic nanoparticles dispersed in aqueous phase via mini-emulsification. Such particles are composed of Donor-Acceptor-Donor (DAD) trimers prepared via Stille coupling, stabilized by amphiphilic block copolymers synthesized by RAFT polymerization. The hydrophilic segment of the block copolymers will not only provide colloidal stability, but also allow for precise control over the surface functionalization. Photocatalytic tests of the resulting particles for H_2 production resulted in promising photocatalytic activity (~ 0.6 mmol g^{-1} h^{-1}). This activity is much enhanced compared to that of DAD trimers dispersed in the water phase without stabilization by the block copolymers.

COMMUNICATION

Global warming, caused by the modern way of human life, has become one of the main challenges for humankind in this century. This has resulted in a climate emergency that warrants strong and immediate action to reduce greenhouse gas emissions. In particular, recent reports from the Intergovernmental Panel on Climate Change (IPCC), a UN organization, emphasize the urgency of taking actions to minimize greenhouse gas emissions, with particular emphasis on energy production, which accounts for the majority of global CO_2 emissions.[1] Investing in renewable energy sources such as solar and wind has become a focal point for several countries globally, aiming to enhance the sustainability of their energy matrix. However, the intermittent nature of such resources is a primary challenge for their full implementation as the main energy source. Various strategies focusing on energy storage have been proposed to overcome this issue. Among these strategies, green H_2 stands out as a promising candidate for solar fuels and their implementation will contribute to the reduction of CO_2 emissions.[2] Green H_2 is mainly produced through the electrolysis of water using renewable energy sources, typically solar or wind. Green H_2 production from solar energy can be divided into two steps: solar energy harvesting using photovoltaic cells, followed by water electrolysis. Alternatively, photocatalytic processes for water splitting offer the advantage of combining both processes within a single system. In this approach, sunlight is initially absorbed by an active material, generating charge carriers, followed by charge separation and transportation. The separated charges (electron/hole) are then transported to water/active material interface, triggering water splitting via redox reactions.[3] Despite its significant promise, the development of efficient photocatalytic systems for H_2 production from water splitting is still pending, representing an urgent need given the escalating demand for low-carbon energy storage.[4-5]

Photocatalytic generation of H_2 through water splitting is typically conducted using inorganic semiconductors, such as TiO_2.[4-6] However, owing to their wide band gap and limited activity at the ultraviolet (UV) region, semi-conducting organic materials, including π-conjugated polymers[7-9] and small organic molecules[10] have emerged as promising alternatives.[11] These materials offer the advantage of covering a broader range of the solar spectrum. The optical properties and the energy positions of the highest occupied molecular orbital (HOMO) and the lowest occupied molecular orbital (LUMO) of these molecules can be easily tuned through adjustments to their chemical structure, resulting in distinct optoelectronic and photocatalytic properties – a feature not as easily attainable with inorganic materials.[11-13] Nevertheless, the efficiency of photocatalytic water splitting is often hindered by the inherent hydrophobicity of organic materials, leading to a small surface area and poor wettability when utilized in bulk. In our previous work,[10] we synthesized a series of conjugated small molecules consisting of donor-acceptor-donor trimers (DAD) via C-C cross coupling reactions. By varying the donor and acceptor moiety, their optoelectronic properties could be easily modulated. Particles composed of these organic trimers were then prepared via nanoprecipitation and their photocatalytic activity was tested for generation of H_2 via water splitting. The best performing system, utilizing (3,4-ethylenedioxythiophene)-benzothiadiazole-(3,4-ethylenedioxythiophene) (EBE), resulted in 275 μmol of H_2 per hour per gram of nanoparticles under UV-visible light irradiation.

Alternatively, conjugated polymer nanoparticles (CPNPs) dispersed in an aqueous phase can also be employed as photocatalysts. Kosco *et al.* reported a successful strategy to prepare organic semiconductor heterojunction nanoparticles formed by donor polymer and acceptor (fullerene or non-fullerene) materials.[7-8] The nanoparticles were stabilized by surfactants, resulting in particles in the nanometric scale, with diameters smaller than 100 nm. Photocatalytic tests using these heterojunction particles resulted in high hydrogen evolution rates with external quantum efficiency up to 8.7% in the visible range (400 to 700 nm). However, in applications involving charge transport such as photocatalytic generation of H_2, the use of surfactant can be detrimental to the final material's performance. The presence of polar groups (*e.g.* sulfate) and counter ions from the surfactants can act as charge traps, drastically decreasing charge mobility.[14] In organic photovoltaic (OPV) applications, strategies to easily remove the surfactant have been proposed to generate functional materials with enhanced charge transport. The best performance to date in OPV applications using nanoparticles was reported by Xie *et al.*[15] The authors developed a strategy to purify the dispersion by employing a temperature-responsive surfactant. The surfactant could be easily removed by centrifugation when the solution was cooled to 0ºC, achieving an impressive efficiency of 7.5%.

The stabilization of particles in aqueous dispersed systems using polymer segments has been extensively studied.[16-17] A very interesting aspect of polymer-stabilized particles lies in the ability to easily control surface functionalization by modifying the composition of the stabilizing segment. With the emergence and widespread adoption of reversible addition–fragmentation chain transfer (RAFT) polymerization, well-defined polymers with controlled molar masses and functionality, while exhibiting sophisticated macromolecular architectures can be readily accessed. The robustness of this process, which can be effectively employed in aqueous dispersed systems, further facilitates the successful design of polymeric nanoparticles with precise control over surface functionalization.[17-19] The customizability of the RAFT technique, operating across a wide range of monomers with diverse functionalities, enables the preparation of various nano-engineered functional particles.[19-20] Moreover, when stimuli-responsive polymer chains are employed to decorate the particle surface, the resulting materials can exhibit CO_2-,[21] thermo- and/or pH- responsive properties[22] expanding their use in a diverse array of applications such as magnetic resonance imaging (MRI),[23] antimicrobial coatings,[24] gene transfection or targeted drug delivery.[22]

Herein, we present a versatile platform designed for the preparation of DAD trimer nanoparticles in aqueous media, stabilized by amphiphilic block copolymers using a soap-free mini-emulsification/solvent evaporation method (Scheme 1). To the best of our knowledge, this is the first report on the use of block copolymers as stabilizers on the stabilization of organic π-conjugated particles for photocatalysis. The DAD trimer, consisting of two thiophene units as electron donors and a benzothiadiazole unit as an electron

acceptor (TBT) was synthesized via Stille cross-coupling reaction. Concurrently, poly(2-(dimethylamino)ethyl methacrylate)-*block*-polystyrene ($PDMAEMA_{39}$-*b*-PS_8) amphiphilic block copolymer was synthesized by RAFT polymerization. The DAD trimer was solubilized in chloroform (organic phase), while the amphiphilic block copolymer was dissolved in the aqueous phase. The two phases were then mixed and subjected to high-energy mixing (ultra-sonication), generating sub-micron size chloroform droplets loaded with DAD trimers, stabilized by PDMAEMA segments (Scheme 1). The solvent was subsequently removed via evaporation, resulting in the DAD trimers nanoparticles dispersed in the aqueous phase. The great customizability of the RAFT process allows not only for precise control over the surface functionalization of the particles, but also for the introduction of functionality to the final particles such as pH-responsiveness. Photocatalytic tests for H_2 production demonstrated promising photocatalytic activity (~ 0.6 mmol g^{-1} h^{-1}) of the resulting nanoengineered particles.

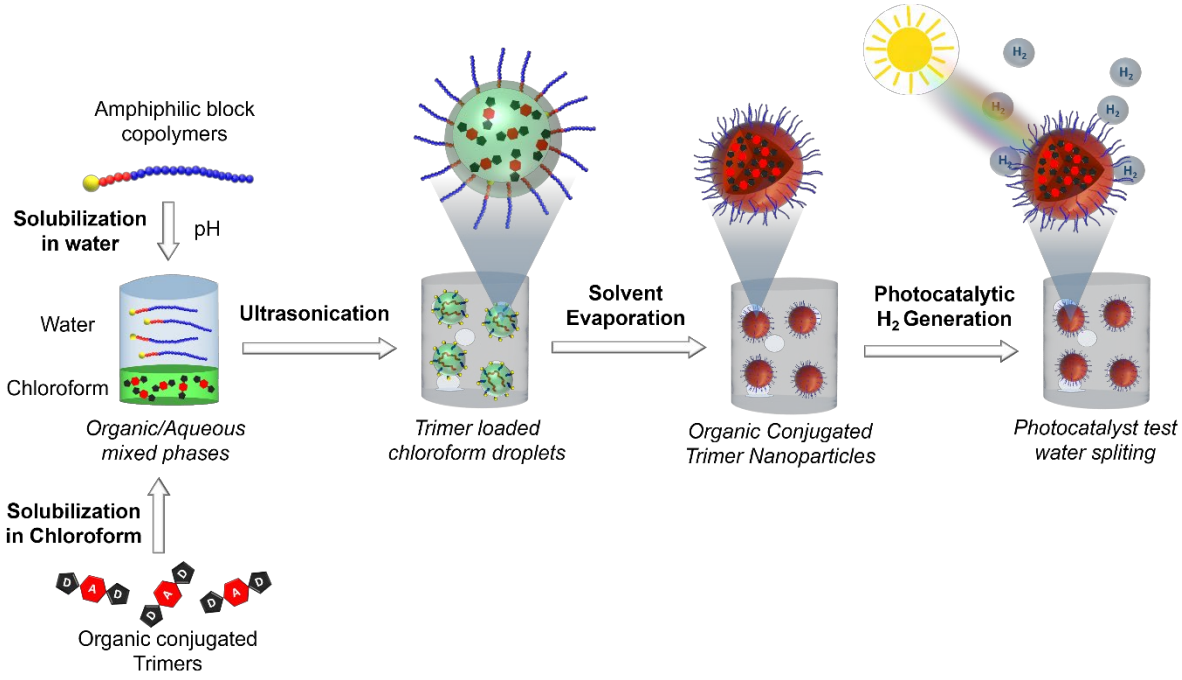

Scheme 1 - General strategy for organic π-conjugated donor-acceptor-donor (DAD) trimer nanoparticles stabilized by amphiphilic block copolymers.

Organic π-conjugated Thiophene-Benzothiadiazole-Thiophene (TBT) was synthesized via Stille cross-coupling reaction, following a modified protocol derived from our previously reported method[10] (see experimental details in SI). TBT was chosen as the DAD trimer due to its good activity in the photocatalytic generation of H_2, as demonstrated in our previous paper.[10] Additionally, this trimer could be easily solubilized in chloroform. For the TBT synthesis, the precursors, dibromo-substituted benzothiadiazole, and a thiophene organotin-derivative, were utilized in the Stille reaction, catalyzed by a Pd-based catalyst (Fig. 1A). Following purification by chromatography column and subsequent recrystallization in methanol, highly pure TBT was yielded (19%) as depicted by the ^{1}H NMR (Fig. 1A and S2). The structure was also confirmed by ^{13}C NMR and Heteronuclear Single Quantum Coherence (HSQC, Fig. S3 and S4). The optical properties of the DAD trimers in THF were explored using UV-visible spectroscopy (Fig. 1B). Two broad, featureless bands were highlighted in the spectrum, one in the near UV region (λ_{max} = 308 nm) and a red-shifted band at λ_{max} = 448 nm (molar absorptivity, ε = 7870 $M^{-1}cm^{-1}$). The optical bandgap of the TBT was determined using a Tauc plot (Fig. S5) resulting in 2.5 eV, in agreement with the optical bandgap obtained in our previous study (2.04 eV for TBT).[10] Additionally, emission and excitation spectra (Fig. 1C) from the DAD trimer solution in THF were recorded at different wavelengths using fluorescence spectroscopy. A significant Stoke's shift in emission was observed (4300 cm^{-1}), a characteristic often seen in dye molecules with push-pull character. These optical properties make TBT an excellent and promising candidate as an active material for the photocatalytic generation of H_2.

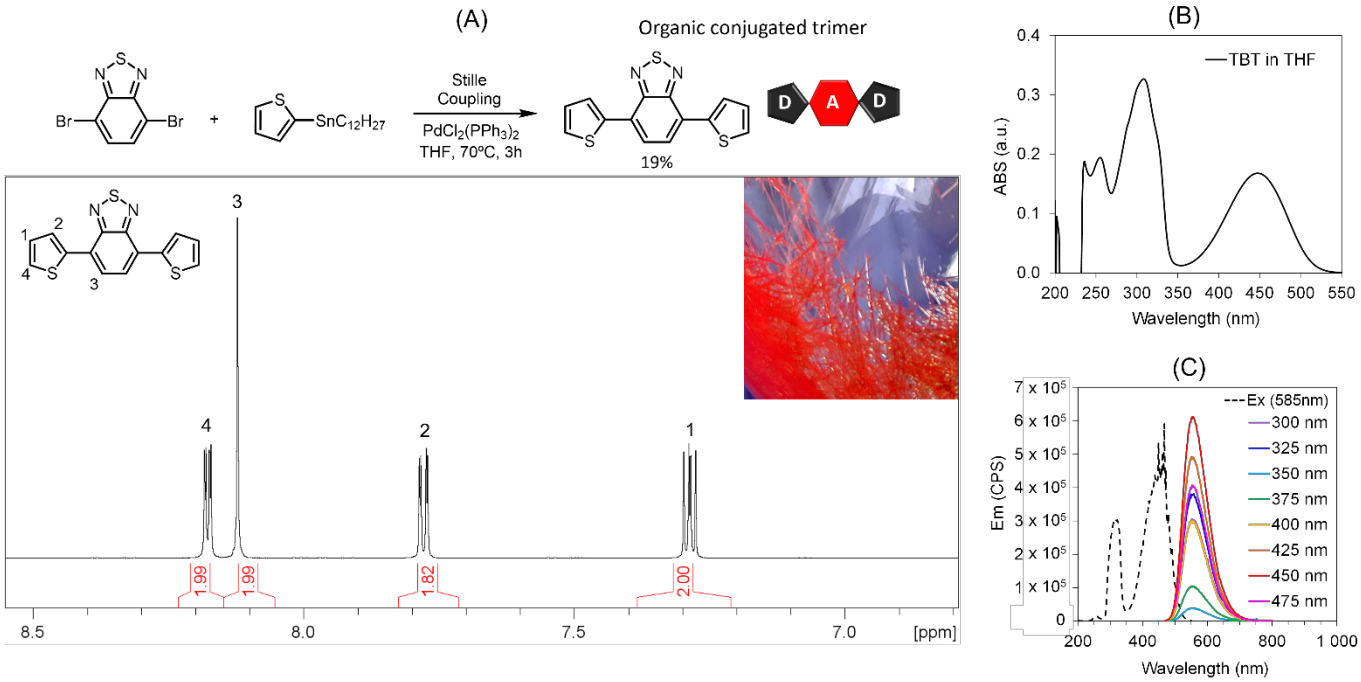

Figure 1 – Synthesis of DAD organic π-conjugated trimer (Thiophene-Benzothiadiazole-Thiophene, TBT) via Stille –cross coupling reaction. (A) Scheme and ^{1}H NMR, 400 MHz, DMSO-d_6, 32 scans; (B) UV spectrum of TBT in THF at 2.1 10^{-5} mol L^{-1} and (C) Spectro fluorescence of TBT in THF at 2.1 10^{-5} mol L^{-1}, excitation spectrum with fixed emission wavelength of 585 nm (dashed-black line, ---) and emission spectra (colored full lines, —) at various excitation wavelengths.

Synthesis of the amphiphilic block copolymer was conducted via a 2-step RAFT solution polymerization using a commercially available trithiocarbonate RAFT agent (^{1}H NMR in Fig. S6). PDMAEMA was selected as the hydrophilic block due to its pH-responsiveness allowing for facile modulation of the surface properties of the particles by simply changing the pH of the medium. Initially, a kinetics study of RAFT polymerization of DMAEMA was undertaken (Fig. S7) with a targeted degree of polymerization (DP) of 80. Subsequently, a second scale-up batch was carried out, and the polymerization was quenched at 49% of conversion. This was conducted to preserve a high degree of livingness to the polymer chains.[25-27] SEC traces (Fig. 2B) show a monomodal peak for PDMAEMA, shifting towards higher molar masses after chain extension reaction with PS. However, due to the short length of the second block (PS), only a slight shift towards higher molar masses was observed. Block formation was then confirmed by DOSY NMR (Fig 2C). As expected, the amphiphilic block copolymer exhibited a lower average diffusion coefficient (1.4 10^{-10} m^2 s^{-1}) than the PDMAEMA-based first block (1.75 10^{-10} m^2 s^{-1}) due to its higher molar mass, confirming the successful formation of the block copolymer. [28-29] In addition, the chemical composition of the block copolymer was analyzed by ^{1}H NMR (Fig. 2D). The degree of polymerization of each block was calculated based on the RAFT-end group ($DP_{PDMAEMA}$ = 35 and DP_{PS} = 7) resulting in a good agreement with the theoretical DP ($DP_{PDMAEMA}$ = 39 and DP_{PS} = 8), calculated based on the monomer conversions obtained for each step of the RAFT polymerization.

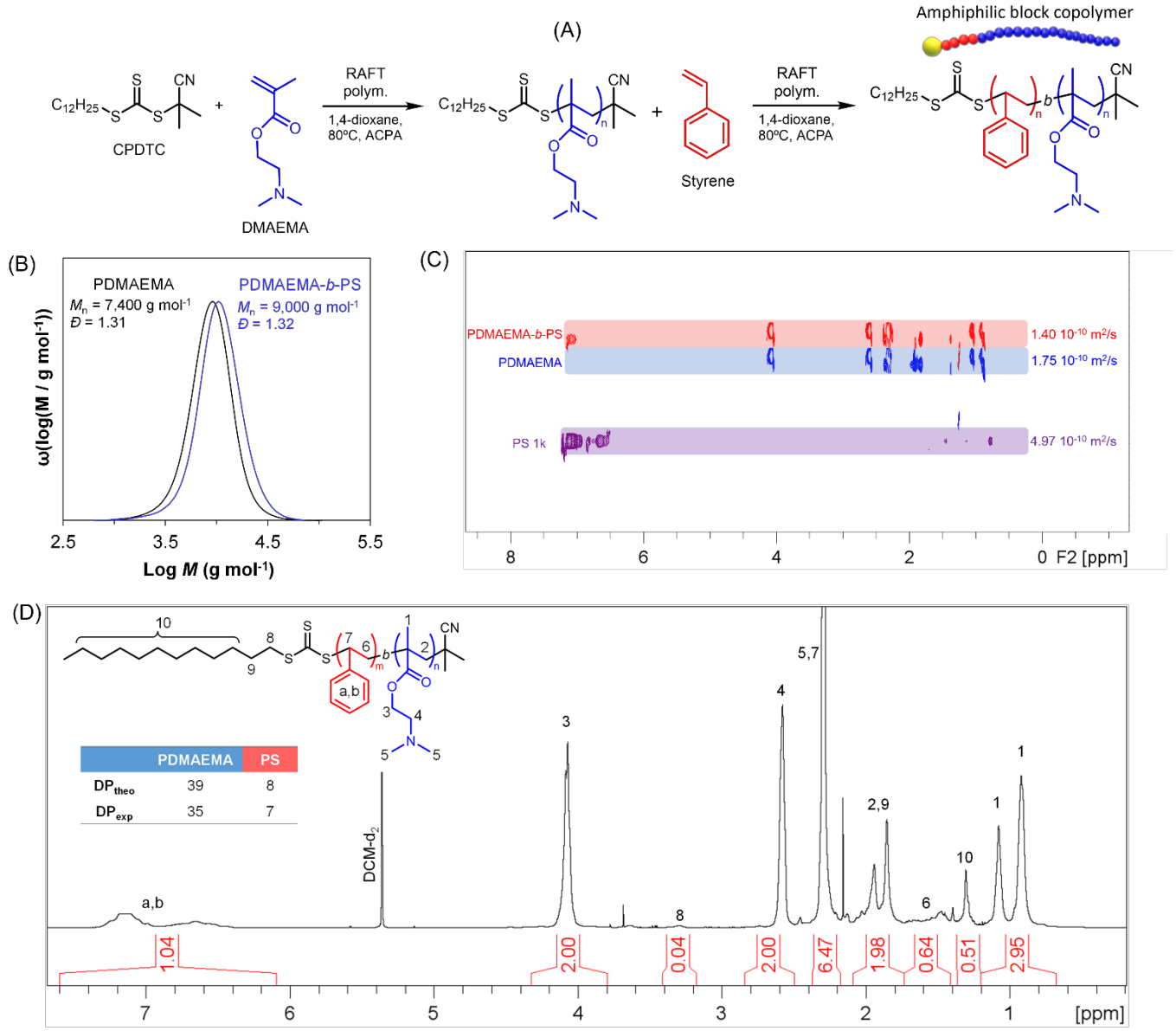

Figure 2 – Synthesis of PDMAEMA$_{39}$-*b*-PS$_8$ via RAFT 2-step solution polymerization. (A) reaction scheme, (B) SEC-chromatograms in DMF of PDMAEMA 1st block (black full line) and PDMAEMA$_{39}$-*b*-PS$_8$ (blue full line), (C) DOSY NMR in $CDCl_3$, 16 scans, 400MHz, of commercial PS 1k (purple), PDMAEMA$_{39}$ 1st block (red) and PDMAEMA$_{39}$-*b*-PS$_8$ block copolymer (blue) and (D) ^{1}H NMR of PDMAEMA$_{39}$-*b*-PS$_8$ in DCM-d$_2$, 400 MHz, 512 scans, the DPs (inset table) were calculated based on the integral of characteristic peak from styrene ($\delta_{a,b}$ = 6.1-7.6 ppm) and DMAEMA (δ_3= 3.8-4.2 ppm) relatively to RAFT-end group (δ_{10}= 1.2-1.3 ppm).

We then shifted our focus on the preparation of particles using a mini-emulsification/solvent evaporation process. This versatile approach has been widely used for the preparation of nanoparticles comprising polymers,[30] proteins,[31-32] inorganic nanoparticles,[25, 33] drugs,[34] etc. In our system, nanoparticles comprising organic π-conjugated trimer (TBT), stabilized by the PDMAEMA$_{39}$-*b*-PS$_8$ were prepared via mini-emulsification (Table 1 and S1). The pH responsiveness of the PDMAEMA segment was exploited to modulate the particle size by simply varying the HCl concentration in the system. At low pH, the tertiary amine side-groups of the PDMAEMA-segment were protonated, resulting in positive charges at the particle surface, contributing to better colloidal stability through electrostatic interactions as evidenced by zeta potential measurements (Fig. 3B). Consequently, a gradual decrease in particle size with the increase of the [HCl]/[PDMAEMA$_{39}$-*b*-PS$_8$] ratio was observed (see Fig. 3A). Controlling particle size is of prime importance for the photocatalytic generation of H_2, as a smaller particle size provides a larger specific surface area for the water splitting reaction to occur at the particle/water interface. Although relatively small particles (Z_{av} < 400 nm, Table 1 and Fig. 3A) were obtained under all conditions studied (NP1-4), particle sedimentation was observed after 48 h. To gain further insight into colloidal stability of particles over time, turbidimetry measurements were conducted (Fig. 3C). Interestingly, the system with an

intermediate [HCl]/[PDMAEMA$_{39}$-*b*-PS$_8$] ratio of 25 (pH 5) exhibited the poorest colloidal stability (NP2 in Fig. 3C). Similar findings of unstable emulsions at intermediate pH (close to pK_a) were reported by other authors[35] in the preparation of W/O (water-in-oil), O/W and multiphasic toluene/water emulsions stabilized by PDMAEMA$_{140}$-*b*-PS$_{50}$. The authors conducted small angle neutron scattering (SANS) and tensiometry experiments, revealing that PDMAEMA segments adopted a flat conformation at oil-water interface with a close to zero spontaneous curvature when pH was close to the pK_a of PDMAEMA (6.5-7.0). This conformation led to unstable emulsions. Although the DP for each block in PDMAEMA$_{140}$-*b*-PS$_{50}$ in their study differs significantly from our system (PDMAEMA$_{39}$-*b*-PS$_8$), it is reasonable to assume a similar behavior in our system, with the chains adopting flat conformation at particle interface at intermediate pH, resulting in unstable emulsions.

Table 1 – TBT nanoparticles stabilized by PDMAEMA$_{39}$-*b*-PS$_8$ prepared via mini-emulsification method.

Run	[HCl]/[MR]	pH$_0$ [b]	Z_{av} (nm)/ *PDI*	ζ-potential (mv)	μ_e (μm cm V^{-1} s^{-1})
NP1	13	6.2	352/0.26	+64.5	+5.1
NP2	25	5.0	288/0.21	+73.8	+5.8
NP3	42	4.5	279/0.29	+72.8	+5.7
NP4	53	3.4	231/0.21	+73.3	+5.8

See detailed experimental section in SI.
MR: PDMAEMA$_{39}$-*b*-PS$_8$ macroRAFT.
μ_e: electrophoretic mobility.

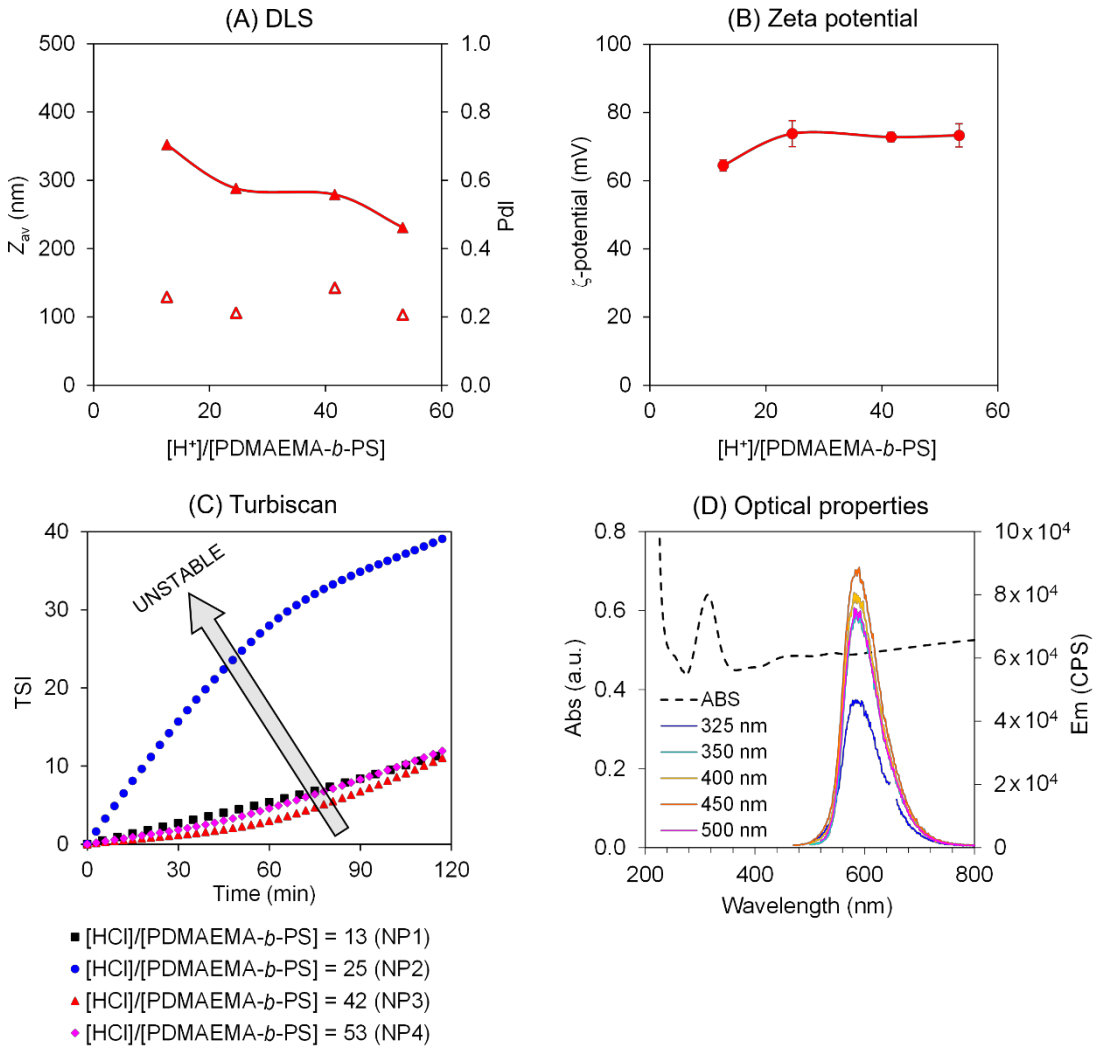

Figure 3 – Preparation of TBT nanoparticles varying the [HCl]/[PDMAEMA$_{39}$-*b*-PS$_8$] ratio. (A) intensity-mean average particle diameter (Z_{av}, filled red triangles) and polydispersity index (PdI, open red triangle) by DLS (NP1-

4), (B) Zeta-potential measurements (ζ) conducted in water at 0.025 g L^{-1}, the pH of the aqueous medium for each sample was pre-adjusted with HCl to match that of the nanoparticle dispersions prior to the dilution (pH_0 in Table 1), (C) turbidimetry via Turbiscan measurements, (D) UV-vis absorption spectrum (dashed black line, ---) and fluorescence emission spectra (full lines, —) of nanoparticles (NP3) with excitation wavelength of 325, 350, 400, 450 and 500nm.

The optical properties of the DAD trimer nanoparticles dispersed in the aqueous phase were also investigated using UV-visible and fluorescence spectroscopies (Fig. 3D). UV-visible spectroscopy revealed a prominent band with a λ_{max} at 314 nm. The spectrum exhibited a large offset from the baseline, indicative of significant scattering from the nanoparticles. Additionally, fluorescence spectroscopy in emission mode was conducted at various excitation wavelengths (Fig. 3D). Remarkably strong fluorescence signals, with a λ_{max} around 590 nm, were observed from the nanoparticles across the range of excitation wavelengths studied. In summary, we have successfully demonstrated the application of our versatile approach in the preparation of nanoparticles composed of organic π-conjugated trimers stabilized by amphiphilic block copolymers, exhibiting distinct and robust fluorescent properties.

The synthesized particles were then used for photocatalytic generation of H_2 (Table S2). For this purpose, 0.1 mL of nanoparticle dispersion (2.5-3.5 g L^{-1}) was dispersed in 20 mL of water/scavenger mixture (vol/vol = 80/20), transferred to a quartz reactor, deoxygenated with Ar, and irradiated under 150 W Hg lamps for 4 h, positioned at 10 cm from the reactor. Initially, the use of different hole scavengers was tested, including methanol, triethanolamine (TEOA) and ascorbic acid (Fig. 4A). TEOA was the only system to effectively generate H_2, while poor H_2 generation was observed for the other two scavengers. This can be attributed to the different pH conditions; the system with TEOA resulted in basic pH (pH 11, PC1), leading to the deprotonation of the PDMAEMA units resulting in steric stabilization of the colloids. Surprisingly, electrophoretic mobility measurements showed negative values under these conditions (-2.4 µm cm V^{-1} s^{-1}, Fig. S8), which can be attributed to the partial hydrolysis of DMAEMA units resulting in carboxylic acid functions.[36] For clarity, these results were expressed in terms of electrophoretic mobility rather than zeta potential, as different media were used for the measurements mimicking the photocatalytic systems. The dielectric constants for such complex media are scarcely available in the literature, which could lead to an inaccurate estimation of the zeta potential values. In contrast with the TEOA system, nanoparticles dispersed in methanol (MeOH) and ascorbic acid aqueous solutions, with slightly acidic and acidic pHs (pH 6.0 and 3.2, respectively), resulted in positive electrophoretic mobilities (+4.8 µm cm V^{-1} s^{-1}, Fig. S8). At such pH levels, the protonation of tertiary amine groups from PDMAEMA is expected, leading to the formation of electrostatic charges at the particle surface. It is well-documented in the literature that electrostatic charges at particle surfaces create charge traps in the final photo-/electro-active material, drastically decreasing the charge transport,[14-15] and consequently, quenching the photocatalytic activity of nanoparticles (Fig. 4A).

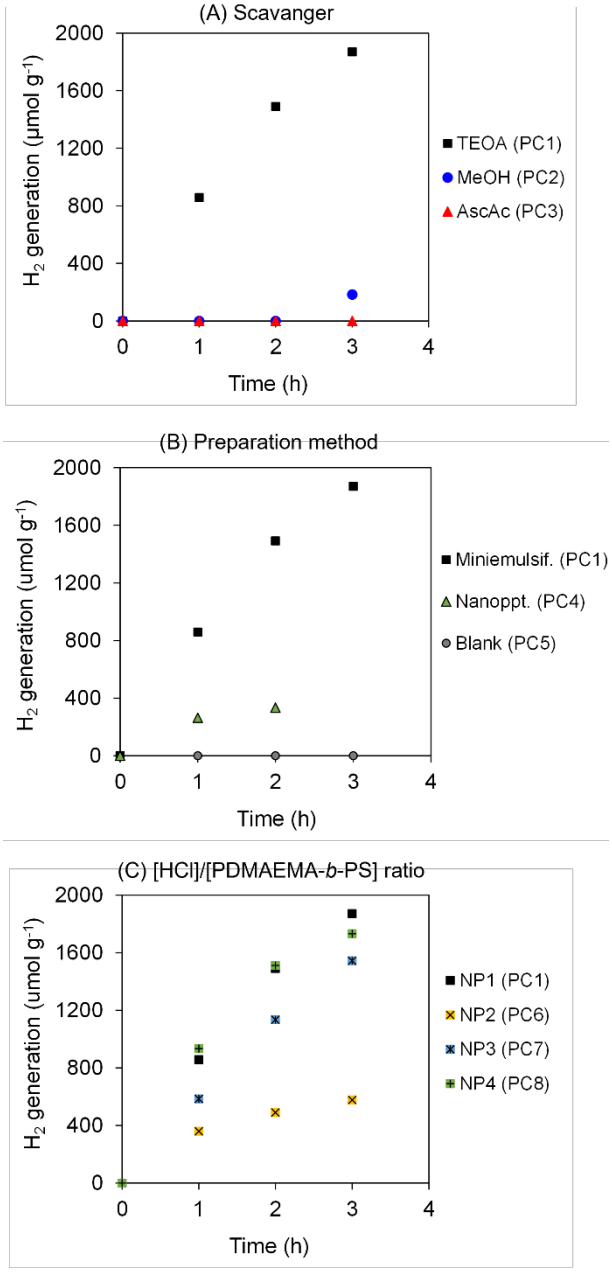

Figure 4 – Photocatalytic test using the TBT nanoparticles stabilized by $PDMAEMA_{39}$-*b*-PS_8. Parameter varied: (A) Scavenger, (B) Preparation method and (C) nanoparticles prepared at different [HCl]/[PDMAEMA-*b*-PS] ratio: 13 (NP1), 25 (NP2), 42 (NP3) and 53 (NP4).

Two preparation methods were studied to compare the efficiency of the organic conjugated trimers on H_2 production: mini-emulsification (used in this work, Scheme 1) and nanoprecipitation.[10, 37] Nanoprecipitation had been previously employed by our group to prepare DAD trimer particles for H_2 production via photocatalysis.[10] This method involves the solubilization of 3 mg of TBT in 5 mL of THF, followed by precipitation in 10 mL of water, with subsequent removal of the solvent (THF) using rotary evaporation. The typical particle diameter observed in such system ranges from 300 nm to 3 µm. The mini-emulsification approach proved to be the most effective method, resulting in the highest H_2 production rate (Fig 4B). This can be attributed to the greater surface area available for H_2 reduction at the water/particle interface due to the small particle size (350 nm, NP1).

Additionally, four nanoparticles prepared at different $[H^+]$/[PDMAEMA-*b*-PS] ratios (NP1-4, Table S1) were tested. It is noteworthy that the protonation degree of the PDMAEMA segments will be dictated by the pH of the scavenger/water medium, employed in a much larger excess (vol/vol = 200/1) than the nanoparticle dispersion volume. Nevertheless, as discussed earlier, varying the $[H^+]$/[PDMAEMA-*b*-PS] ratio during the particle preparation still has a direct impact on the particle size and the colloidal stability (see Fig 3). It is important to highlight that the photocatalytic tests were conducted 11 days after synthesis,

which can be considered long-term for the particles to reach a steady state in terms of particle size evolution over time. High rates of H_2 generation (190-620 μmol g^{-1} h^{-1}, Table S2) were observed in all experiments prepared via mini-emulsification, regardless of the $[H^+]$/[PDMAEMA-*b*-PS] ratio. The lower H_2 generation rate for the nanoparticles prepared with a $[H^+]$/[PDMAEMA-*b*-PS] ratio of 25 (190 μmol g^{-1} h^{-1}) can be associated with the poorer colloidal stability of this system (NP2 in Fig 3B). One might argue that the particles stabilization provided by amphiphilic block copolymers containing unconjugated monomer units such as styrene and DMAEMA - which are known to be charge insulators – would result in very poor photocatalytic activity. However, our results suggest the opposite, with high photocatalytic activity for the particles stabilized with amphiphilic block copolymers. Further photocatalytic tests, including recycling tests, are currently underway and will be reported in a future publication. In summary, our strategy of employing amphiphilic block on the preparation of organic conjugated trimer nanoparticles via mini-emulsification approach resulted in the highest H_2 production rate, with no photocatalytic inhibition due to the use of unconjugated block copolymer as stabilizer. This important result paves the way for the development of the next generation of nanoengineered nanoparticle systems for the photocatalytic generation of hydrogen.

CONCLUSION

The synthesis of organic π-conjugated trimers nanoparticles stabilized by amphiphilic block copolymers for the photocatalytic generation of H_2 was detailed. The mini-emulsification/solvent evaporation method yielded stable particles with diameters ranging from 200 to 300 nm, although some particle precipitation was observed after 48 h. The nanoengineered particles were decorated with pH-responsive segments composed of DMAEMA units, allowing for particle size and hydrophilicity to be readily controlled. The comparison of different preparation methods revealed that particles obtained through mini-emulsification exhibited enhanced photocatalytic activity in H_2 generation (up to 620 μmol g^{-1} h^{-1}) compared to other methods (nanoprecipitation: 170 μmol g^{-1} h^{-1}). This significant finding demonstrates that amphiphilic block copolymers, even with non π-conjugated sequences, can serve as effective stabilizers for nanoparticles containing electronically active materials or molecular (photo)catalysts, specifically for the photocatalytic generation of H_2. This strategy not only provides a robust platform for the synthesis of stable nanoparticles but also lays the foundation for the next generation of environmentally friendly, green, and safe chemical processes for photocatalytic solar fuel generation.

ASSOCIATED CONTENT

Experimental procedures and additional characterization available in Supplementary Information.

AUTHOR INFORMATION

Corresponding Authors

Thiago R. Guimaraes − Univ. Bordeaux, LCPO and ICMCB, CNRS, Bordeaux INP, F-33607 Pessac, France.
orcid.org/0000-0003-0289-5015
Email: thiago.guimaraes@u-bordeaux.fr

Jean-Louis Bobet – Univ. Bordeaux, ICMCB, CNRS, Bordeaux INP, F-33600 Pessac, France.
orcid.org/0000-0001-7838-7004
Email: jean-louis.bobet@icmcb.cnrs.fr

Eric Cloutet – Univ. Bordeaux, LCPO, CNRS, Bordeaux INP, F-33607 Pessac, France.
orcid.org/0000-0002-5616-2979
Email: eric.cloutet@u-bordeaux.fr

Authors
Alisha Khan − Univ. Paris-Saclay, Institut de Chimie Physique (UMR 8000), CNRS, Orsay 91405, France.
orcid.org/0009-0002-8451-6946

Hynd Remita − Univ. Paris-Saclay, Institut de Chimie Physique (UMR 8000), CNRS, Orsay 91405, France.
orcid.org/0000-0003-3698-9327

Author Contributions
The manuscript was written through contributions of all authors. All authors have given approval to the final version of the manuscript.

ACKNOWLEDGMENT
The authors are grateful for the grant "Grands Programmes de Recherche, Post Petroleum Materials-PPM" from the University of Bordeaux. The authors also thank Léna Alembik for the DOSY NMR measurements and Mélanie Bousquet for their help with the SEC analysis.

REFERENCES

[1] H. Lee, K. Calvin, D. Dasgupta, G. Krinner, A. Mukherji, P. Thorne, C. Trisos, J. Romero, P. Aldunce, K. Barret, **2023**.
[2] A. M. Oliveira, R. R. Beswick, Y. S. Yan, *Current Opinion in Chemical Engineering* **2021**, *33*, 100701.
[3] M. V. Pavliuk, S. Wrede, A. Liu, A. Brnovic, S. Wang, M. Axelsson, H. Tian, *Chem Soc Rev* **2022**, *51*, 6909-6935.
[4] G. Zhang, Z. A. Lan, X. Wang, *Angew Chem Int Ed Engl* **2016**, *55*, 15712-15727.
[5] A. Wadsworth, Z. Hamid, J. Kosco, N. Gasparini, I. McCulloch, *Adv Mater* **2020**, *32*, e2001763.
[6] A. Fujishima, K. Honda, *nature* **1972**, *238*, 37-38.
[7] J. Kosco, M. Bidwell, H. Cha, T. Martin, C. T. Howells, M. Sachs, D. H. Anjum, S. Gonzalez Lopez, L. Zou, A. Wadsworth, W. Zhang, L. Zhang, J. Tellam, R. Sougrat, F. Laquai, D. M. DeLongchamp, J. R. Durrant, I. McCulloch, *Nat Mater* **2020**, *19*, 559-565.
[8] J. Kosco, S. Gonzalez-Carrero, C. T. Howells, T. Fei, Y. F. Dong, R. Sougrat, G. T. Harrison, Y. Firdaus, R. Sheelamanthula, B. Purushothaman, F. Moruzzi, W. D. Xu, L. Y. Zhao, A. Basu, S. De Wolf, T. D. Anthopoulos, J. R. Durrant, I. McCulloch, *Nature Energy* **2022**, *7*, 340-351.
[9] X. Yuan, D. Dragoe, P. Beaunier, D. B. Uribe, L. Ramos, M. G. Méndez-Medrano, H. Remita, *Journal of Materials Chemistry A* **2020**, *8*, 268-277.
[10] X. J. Yuan, C. Wang, L. Vallan, A. T. Bui, G. Jonusauskas, N. D. McClenaghan, C. Grazon, S. Lacomme, C. Brochon, H. Remita, G. Hadziioannou, E. Cloutet, *Advanced Functional Materials* **2023**, *33*, 2211730.
[11] J. Kosco, F. Moruzzi, B. Willner, I. McCulloch, *Advanced Energy Materials* **2020**, *10*, 2001935.
[12] Y. O. Wang, A. Vogel, M. Sachs, R. S. Sprick, L. Wilbraham, S. J. A. Moniz, R. Godin, M. A. Zwijnenburg, J. R. Durrant, A. I. Cooper, J. W. Tang, *Nature Energy* **2019**, *4*, 746-760.
[13] X. Yuan, K. Yang, C. Grazon, C. Wang, L. Vallan, J. D. Isasa, P. M. Resende, F. Li, C. Brochon, H. Remita, G. Hadziioannou, E. Cloutet, J. Li, *Angew Chem Int Ed Engl* **2023**, e202315333.
[14] L. Parrenin, G. Laurans, E. Pavlopoulou, G. Fleury, G. Pecastaings, C. Brochon, L. Vignau, G. Hadziioannou, E. Cloutet, *Langmuir* **2017**, *33*, 1507-1515.
[15] C. Xie, T. Heumuller, W. Gruber, X. Tang, A. Classen, I. Schuldes, M. Bidwell, A. Spath, R. H. Fink, T. Unruh, I. McCulloch, N. Li, C. J. Brabec, *Nat Commun* **2018**, *9*, 5335.
[16] M. Karimi, A. Ghasemi, P. S. Zangabad, R. Rahighi, S. M. M. Basri, H. Mirshekari, M. Amiri, Z. S. Pishabad, A. Aslani, M. Bozorgomid, *Chem. Soc. Rev.* **2016**, *45*, 1457-1501.
[17] D. Le, D. Keller, G. Delaittre, *Macromol. Rapid Commun.* **2019**, *40*, 1800551.
[18] D. J. Keddie, *Chem. Soc. Rev.* **2014**, *43*, 496-505.
[19] P. B. Zetterlund, S. C. Thickett, S. b. Perrier, E. Bourgeat-Lami, M. Lansalot, *Chem. Rev.* **2015**, *115*, 9745-9800.
[20] M. Lansalot, J. Rieger, F. D'Agosto, *Macromolecular Self-assembly* **2016**, 33-82.
[21] Q. Zhang, G. Yu, W.-J. Wang, H. Yuan, B.-G. Li, S. Zhu, *Macromolecules* **2013**, *46*, 1261-1267.

[22] M. A. C. Stuart, W. T. Huck, J. Genzer, M. Müller, C. Ober, M. Stamm, G. B. Sukhorukov, I. Szleifer, V. V. Tsukruk, M. Urban, *Nat. Mater.* **2010**, *9*, 101-113.
[23] C. Zhang, D. S. Kim, J. Lawrence, C. J. Hawker, A. K. Whittaker, *ACS Macro Letters* **2018**, *7*, 921-926.
[24] M. Williams, N. Penfold, J. Lovett, N. Warren, C. Douglas, N. Doroshenko, P. Verstraete, J. Smets, S. Armes, *Polym. Chem.* **2016**, *7*, 3864-3873.
[25] T. R. Guimarães, M. Lansalot, E. Bourgeat-Lami, *Polymer Chemistry* **2020**, *11*, 648-652.
[26] D. J. Keddie, *Chem Soc Rev* **2014**, *43*, 496-505.
[27] G. Moad, E. Rizzardo, *RAFT Polymerization: Methods, Synthesis, and Applications*, John Wiley & Sons, **2021**.
[28] P. J. Voorter, M. Wagner, C. Rosenauer, J. H. Dai, P. Subramanian, A. Mckay, N. R. Cameron, J. J. Michels, T. Junkers, *Polymer Chemistry* **2023**, *14*, 5140-5146.
[29] K. Philipps, T. Junkers, J. J. Michels, *Polymer Chemistry* **2021**, *12*, 2522-2531.
[30] L. R. MacFarlane, H. Shaikh, J. D. Garcia-Hernandez, M. Vespa, T. Fukui, I. Manners, *Nature Reviews Materials* **2021**, *6*, 7-26.
[31] M. Fach, L. Radi, P. R. Wich, *J Am Chem Soc* **2016**, *138*, 14820-14823.
[32] J. Kaltbeitzel, P. R. Wich, *Angew Chem Int Ed Engl* **2023**, *62*, e202216097.
[33] T. R. Guimarães, M. Lansalot, E. Bourgeat-Lami, *Journal of Materials Chemistry B* **2020**, *8*, 4917-4929.
[34] N. Anton, J. P. Benoit, P. Saulnier, *J Control Release* **2008**, *128*, 185-199.
[35] L. Besnard, M. Protat, F. Malloggi, J. Daillant, F. Cousin, N. Pantoustier, P. Guenoun, P. Perrin, *Soft Matter* **2014**, *10*, 7073-7087.
[36] P. Van de Wetering, N. Zuidam, M. Van Steenbergen, O. Van der Houwen, W. Underberg, W. Hennink, *Macromolecules* **1998**, *31*, 8063-8068.
[37] G. Prunet, L. Parrenin, E. Pavlopoulou, G. Pecastaings, C. Brochon, G. Hadziioannou, E. Cloutet, *Macromolecular Rapid Communications* **2018**, *39*, 1700504.